Distributed thermoelectric model of a PV module: effect of inhomogeneous boundary conditions

Fadi BOURARACH[1*]**, Arttu TUOMIRANTA**[2]**, Stéphane GIBOUT**[1]

[1] Universite de Pau et des Pays de l'Adour, E2S UPPA, LaTEP, Pau, France
[2] TotalEnergies One Tech, TSA 12142, 59779 LILLE CEDEX FRANCE
* (Corresponding author: fadi.bourarach@univ-pau.fr)

Abstract - A distributed thermoelectric model for photovoltaic (PV) modules is introduced, incorporating comprehensive heat transfer modes, electrical coupling, and spatially resolved convective heat transfer coefficients. Validated against the SANDIA model, this model accurately captures temperature distribution and power loss due to inhomogeneous convective boundary conditions. It serves as a precursor to a more intricate aerodynamic model, aiming to refine PV performance predictions and inform the design of new PV installations, particularly in aquatic settings or with innovative geometries.

Nomenclature

λ	Thermal conductivity , W/m.K	h_{coef}	Convectif heat exchange coef , W/m^2.K
C	Thermal capacity , J/kg.K		Subscripts & superscripts
ρ	Density , kg/m^3	$()_f$	front
e	Thickness' layer , m	$()_b$	back
T	Temperature , K	$()_{0-4}$	layer's index
V	Volume , m^3	$()_{conv}$	convective
Δt	Timestep , s	$()_{cond}$	conductive
Φ	Heat flux , W	$()_{rad\,shor}$	radiative, short wavelength
η	PV cell's efficiency , %	$()_{rad\,long}$	radiative, long wavelength
β	Temperature coefficient , %/°C	$()^i$	at timestep i

1. Introduction

The scarcity of available sites for classical ground-mounted solar PV, due to the low power density [1], leads to the emergence of new PV systems aimed at resolving conflicts with residential and agricultural needs [2, 3] as part of SDG 7 [4]. (From the Atlas of Sustainable Development Goals. Goal number 7: affordable & clean energy - Access to universal and sustainable electricity). Precise modeling of photovoltaic (PV) panel performance necessitates knowledge of its cell temperature. Predicting this temperature becomes progressively more challenging due to new design features of PV installations [3, 5, 6], the latter impacting their yield and therefore their return on investment.

The top two factors influencing the electrical output of a PV module are irradiation and temperature [7, 8], mainly because the diode model parameters are primarily influenced by irradiation and temperature. The evolution of thermal models for PV systems has significantly progressed over time, with each contribution aimed at addressing specific limitations and challenges. Beginning with a simplified one-layer model proposed in 1987 [9], subsequent developments have introduced increasingly complex approaches. In 2010, an electrical analogy-based six-layer model was introduced, albeit neglecting radiative heat transfer [10]. This was followed by the development of a transient one-layer model in 2014, focusing on estimating module temperature [11]. Further advancements in 2020 included the introduction of a one-layer model with forced water cooling [12] and a three-layer model addressing linearization challenges [13]. However, both of these models were noted to be time-consuming, prompting the proposal of regression models. In 2021, a three-layer model with water cooling and an electrical analogy

was introduced [14], yet still facing similar time-consuming issues. The most recent development in 2023 involved a transient electrical five-layer model, focusing on second-to-minute timescales but encountering the need to linearize radiative heat transfer equations [15]. These chronological advancements highlight a progression toward more sophisticated thermal models for PV systems, with an ongoing emphasis on capturing dynamic behavior while overcoming methodological challenges.

All the revised thermal model articles include the convective heat transfer coefficient (h_{coef}) from correlations to estimate the average heat transfer on the entire module. Several studies show a varying distribution of h_{coef} on the PV installation depending on its geometrical configuration [6, 16–18]. One study in particular [18] shows that the inhomogeneity of the h_{coef} can vary within $\pm 40\%$, which leads to mitigated cell temperature estimations [5]. This implies the necessity to explore more advanced thermal approaches that use a local instead of an average h_{coef} value and ultimately an aerodynamic model for PV installations.

The proposed thermal model will, at a first step, use the same correlation to estimate the average h_{coef} on the entire module and roughly estimate its inhomogeneity on each cell. The innovation is in the possibility to include local h_{coef} on each cell to include the thermal boundary layer on the top and back surface of the module following [18] estimations on the h_{coef}. This work is a bridge towards a new generation of thermal models that include distributed thermal boundary layer on the top and back surface of the module. The electrical coupling will be taken in two folds. Firstly, the temperature of the cell influences directly its efficiency. Secondly, due to the series electrical layout of the module's substring, the cell with the lowest efficiency will hinder the entire substring. The goal of this paper is to show that inhomogeneous convective boundary conditions have a noticeable impact on the real production of the PV module.

2. Material and methods

A 3D coupled five-layer transient physical finite-volume model is introduced, incorporating a local distribution of h_{coef} as input. The thermo-electrical coupling is included in two folds: the classical thermal effect on the cell's efficiency and the substring effect. Indeed, the current of the lowest PV cell production will impact the entire module due to the substring's electrical layout. This electrical coupling is essential for the estimation of the impact of the inhomogeneity on the entire module. The model is developed using Python and will be validated numerically, followed by a study using field data. The validation will compare the proposed model with the validated SANDIA one-layer model [9]. The study will use field data provided by QEERI (Qatar Environment and Energy Research Institute: a collaborator of TotalEnergies). Not focusing on the calculation of the h_{coef}, the electrical power loss due to the non-homogeneous h_{coef} distribution, affecting the PV's electrical production, will be estimated as a first step.

2.1. Description and hypotheses

The proposed physical model includes all three modes of heat transfer mechanisms, namely conduction, convection, and radiation. As seen in Figure 1, the conduction occurs inside the module both on the Z-axis (main dissipation axis) and in the XY-axes (secondary dissipation axes). The convection occurs between the front and back surface temperatures and the ambient air temperature (T_{air}). The infrared radiation is included between the front and back modules with the sky's temperatures (T_{sky}) and the substrate's temperature (T_{sub}). Each infrared radiation flux is associated with its corresponding thermal view factor. The substrate can be ground, water, or any other material below the PV modules.

The side edges of the module, are considered adiabatic as a first approximation. This assumption is justified by the fact that the main axis of dissipation is considered to be the Z-axis. Indeed, the surface exchange of the Z-axis dissipation is much larger than the surface exchange of the XY-axes.

The temperature of each layer of the 3D discretized PV module is assumed to have a homogeneous temperature profile. Each layer is defined by its thickness, thermal conductivity, and thermal capacity. The incident irradiation on the PV cells passes through the front glass and the front encapsulant before reaching the PV cell. The individual optical properties of each layer are encompassed in one coefficient: reflectivity.
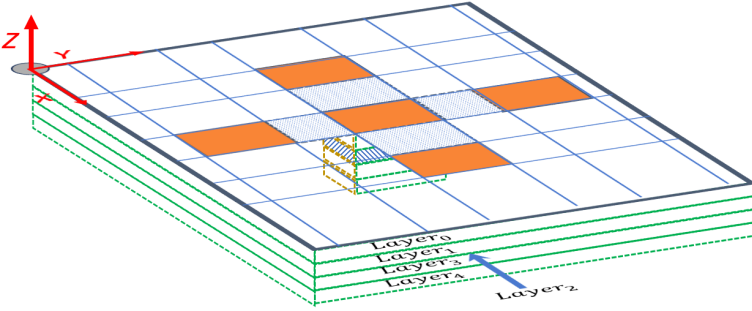
2.2. Discretization

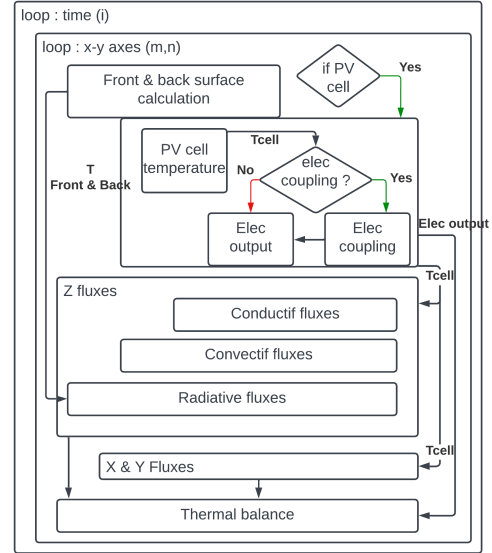Figure 1: Spatial discretization of a PV module

Figure 2: Resolution algorithm

As shown in Figure 1, the 3D thermal model discretizes the XY-axes into blocks named pv-cell-blocks and non-cell-blocks respectively in orange and dotted. The pv-cell-blocks contain five layers in the Z direction, in the following order: front glass, front encapsulant, PV cell, back encapsulant, back glass/backsheet. The non-cell-blocks are similar to the pv-cell-blocks except they contain four layers, omitting the PV cell layer.

An explicit time discretization (with a variable time step) is used, resulting in (1). The equation is discretized spatially in the three axes XYZ using respectively the indices m, n, and k, and temporally using the index i. ρ is the density, λ is the thermal conductivity, C is the thermal capacity, V is the volume, $T_{m,n,k}^{i+1} - T_{m,n,k}^{i}$ is the temperature difference between the timestamps i and $i+1$, and Δt is the timestep separating these timestamps.

$$T_{m,n,k}^{i+1} = T_{m,n,k}^{i} + \frac{\sum_{m,n,k} \Phi(T_{m,n,k}^{i})}{\rho_{m,n,k}.C_{m,n,k}.V_{m,n,k}}.\Delta t \tag{1}$$

$$\Phi_{x+} + \Phi_{x-} + \Phi_{y+} + \Phi_{y-} = \Phi_{lateral} \tag{2}$$

2.3. Thermal fluxes and balance

The XY-axes fluxes contain only conduction. A detailed dive of the classical law of heat conduction will be omitted, also known as Fourier's law equation. As shown in Equation (2), all lateral fluxes, for a node m, n, k, will be summed into a single flux for simplification, $\phi_{lateral}$, neglecting the refraction loss.

The Z-axis will contain most of the dissipation fluxes as well as the heating source coming from the sun's short wavelength irradiation. In Figure 3, the fluxes are categorized into

conduction, convection, electric, short, and long irradiation. For a pv-cell-block, the PV cell will receive short wavelength irradiation from the sun. Except for the interface extremities (air front-surface & air back-surface), the optical losses due to reflection (and refraction) in the layer enveloping the PV cell will be ignored for this study. Part of the sun's irradiation energy will be converted into electrical energy, ϕ_{elec} (3) & (4), where, η_{std} is the PV cell efficiency at standard test conditions (STC), β is the temperature dependence of the PV cell efficiency, T_{ref}, is the reference temperature used at STC, T_{cell}, is the PV cell temperature, and η is the newly calculated PV cell efficiency. The leftover energy will be dissipated into heat. This heat will have to pass through the four layers as conduction to reach the front and the back surface of the pv-cell-block.

$$\eta = \eta_{stc} * (1 - \beta * (T_{cell} - T_{ref})) \tag{3}$$

$$\phi_{elec} = \phi_{rad\,short} * \eta \tag{4}$$

On the surfaces of the PV module, convection and radiation take over the dissipation. The convection occurs between the front and back surfaces and the ambient air temperature. For radiative exchanges, both the front and the back are assigned thermal view factors for both the sky and substrate. The temperature of the ground is assumed to be equal to the ambient temperature, and the sky temperature is taken as a rough approximation $T_{\text{sky}} = T_{\text{ambient}}$. The T_{sky} has a non-negligible impact on the final T_{cell} estimation [19]. The main goal of this paper being to demonstrate the effect of an inhomogeneous h_{coef}, the sky temperature model can be overseen as long as both models (Proposed and SANDIA) use the same correlation. Both T_{sky} and T_{sub} models can be changed on demand with a more reliable one. The thermal parameters used for the simulation are described in Table 1. For a non-cell-block, all the mechanisms remain except for the existence of the PV cell, leading to no het source and to direct contact of the front and back encapsulant: $\phi_{\text{cond}\,1\to2}$ and $\phi_{\text{cond}\,2\to3}$ are replaced by $\phi_{\text{cond}\,1\to3}$.

2.4. Resolution

The finite volume method was employed for resolving the equations. For each volume element, all the XYZ-axes fluxes are calculated. These fluxes are injected into the discretized thermal heat balance equation (1). Figure 2 explains the algorithm used for the resolution. For each timestep, the initial step involves calculating the front and back surface temperatures using flux continuity on the front and back boundaries (with nonlinear radiative heat transfer equations). The convective flux is also included as well as the conduction from the half front and back layers to their respective surfaces. Then, the iteration is performed over the different XY blocks/axes, and all the XYZ fluxes are calculated. This step contains only conduction fluxes.

3. Results and validation

To validate the dynamic behavior, a simulation will be introduced using a single cell (i.e. $m_{\text{Max}} = 1$, $n_{\text{Max}} = 1$). The results will be compared agains the SANDIA model [9] as it uses similar inputs as the proposed model. It assumes one cell covering the entire PV module's surface, modeled as a single layer, thus neglecting the conduction mechanism. A constant h_{coef} is applied to each surface independently, which facilitates the validation procedure.

3.1. Validation of the temperature's dynamic behaviour

Let's consider the following case: a single PV cell laid flat (tilt $= 0°$). The thermal parameters of each layer are detailed in Table 1. The module is irradiated with $1000\,[\text{W/m}^2]$ at $t = 0$. The front surface faces towards the sky, and the rear surface towards the substrate. This
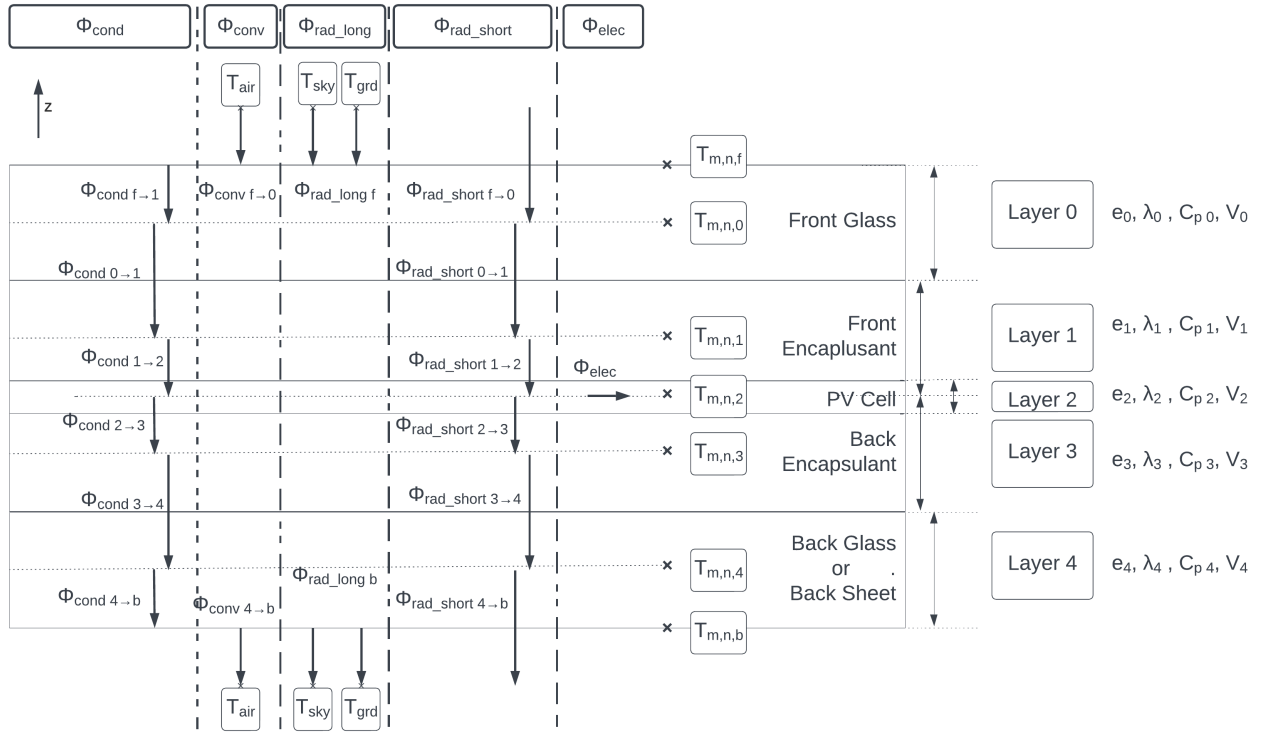
Figure 3: Flux representation of all 3 thermal tranfer modes for a pv-cell-block.

	λ	C	ρ	e
	$W/K.m$	$J/kg.K$	kg/m^3	mm
Front glass	1.7	800	2500	2
Front encapsulant	0.24	1400	940	1
PV cell	1.26e3	700	2328	0.1
Back encapsulant	0.24	1400	940	1
Back glass	1.7	800	2500	1

Table 1: Thermal parameters used for simulations
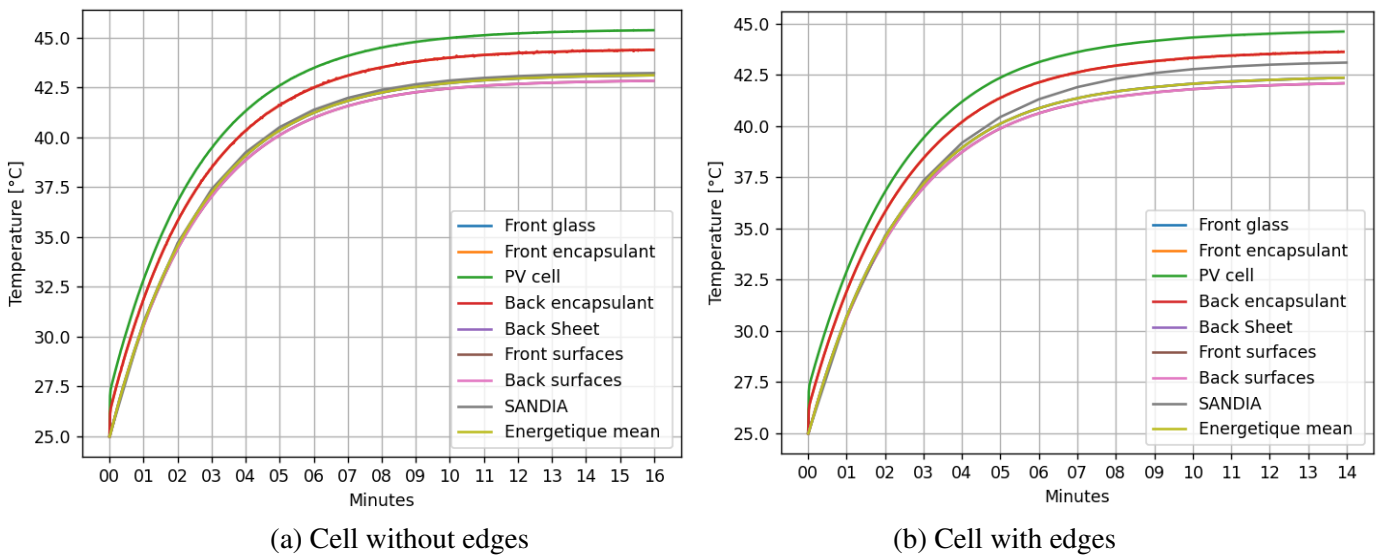

(a) Cell without edges

(b) Cell with edges

Figure 4: Dynamic thermal simulation of a pv cell: (a) with the 5-layer only, (b) with a 4-layered block (without cell) surrounding the 5-layer pv-cell-lock.

implies that the front and rear sky view factors used in the radiative surface heat exchanges are respectively 1 and 0, inversely for the front and rear substrate view factors. A constant air temperature of 25°C, and front and back h_{coef} of $20 \, [\text{W/m}^2\text{K}]$ are applied. $T_{\text{sky}} = T_{\text{ambient}}$ changes with respect to the climatic conditions [20].

$$T_{(m,n) \, weighted \, average} = \frac{\sum_k \rho_k . C_k . V_k . T_k}{\sum_k \rho_k . C_k . V_k} \quad (5)$$

In Figure 4, the results of two simulations are displayed, namely the "pv-cell-block alone" and the "pv-cell-block surrounded with non-cell-blocks". The graphs represent the evolution of temperature through time. The lines represent the temperature evolution of each layer of the proposed thermal model and the SANDIA model, where an energetic mean temperature was conducted as a post-process using (5) to compare the two models (one-layer & five-layer).

In Figure 4a, it can be observed that the dynamic behavior of the proposed model matches SANDIA's. The calculated cell temperatures for both models have a discrepancy which is caused by the internal conduction in the PV module. The energetic mean confirms this assumption. Indeed, the latter coincides with the SANDIA's model. In Figure 4b, a slight change can be observed in the behavior of the proposed model due to the non-cell-blocks. This difference is explained by the difference between the new boundary exchange surfaces of the pv-cell-block and the adiabatic ones. This change is also reflected in the energetic mean.

3.2. Study using field inputs

The final goal of the proposed model is to predict the cell's temperature in a utility-scale PV power plant. The h_{coef} varies globally within the PV module rows and locally on the PV module level. Three simulations were conducted to evaluate the electrical impact of the non-homogeneity of the h_{coef}. The simulations consist of 20 cells, 2 in the y-axis and 10 in the x-axis, representing a classic PV module substring. Two simulations were conducted using SANDIA's model as a reference and the proposed model using a constant front and back h_{coef}. In contrast, in the third simulation, a spatial variation of the h_{coef} is imposed in the x-direction, using the proposed model, following the [18] results: $\pm 40\%$. The surface average of the spatial variation of the h_{coef} is equivalent to the constant h_{coef} imposed in the previous simulations. The leading edge of the substring will be downshifted by -20%, and the trailing edge will be increased by $+20\%$. The intermediate values will follow a linear interpolation. Each XY element will have a constant h_{coef} value. Due to confidentiality reasons, the meteorological data used in this study will not be provided in this paper.

Both models use the same electrical coupling. The efficiency drop is calculated using Equation (3) to calculate the electric flux at time i, ϕ_{elec}^i. The electrical coupling is extended to the substring level. Indeed, since the PV cells are connected in series, their working point is hindered by the cell that generates the least current. This behavior is modeled by setting the efficiency of all cells using the highest cell temperature of the substring.

Figure 5 represents a simulation using QEERI's data for one clear sky day. It is observed in both 5a and 5b that SANDIA produces the most power and energy. As expected, the simulation with the spatial variation of the h_{coef} is producing the least. Sub-figure 5a displays the power output of the 20 cells PV module. A noticeable difference in power between the three simulations is seen. SANDIA's model produces the most, followed by the constant h_{coef} and then the spatially resolved imposed h_{coef}. In Sub-Figure 5b, the energy computation is presented for the three cases. SANDIA's model overestimates the proposed model with a constant h_{coef} by $+7.58\%$ and $+9.58\%$ for the proposed model with the spatially resolved h_{coef}. The relative difference between the two simulations using the proposed model is 2.16%.
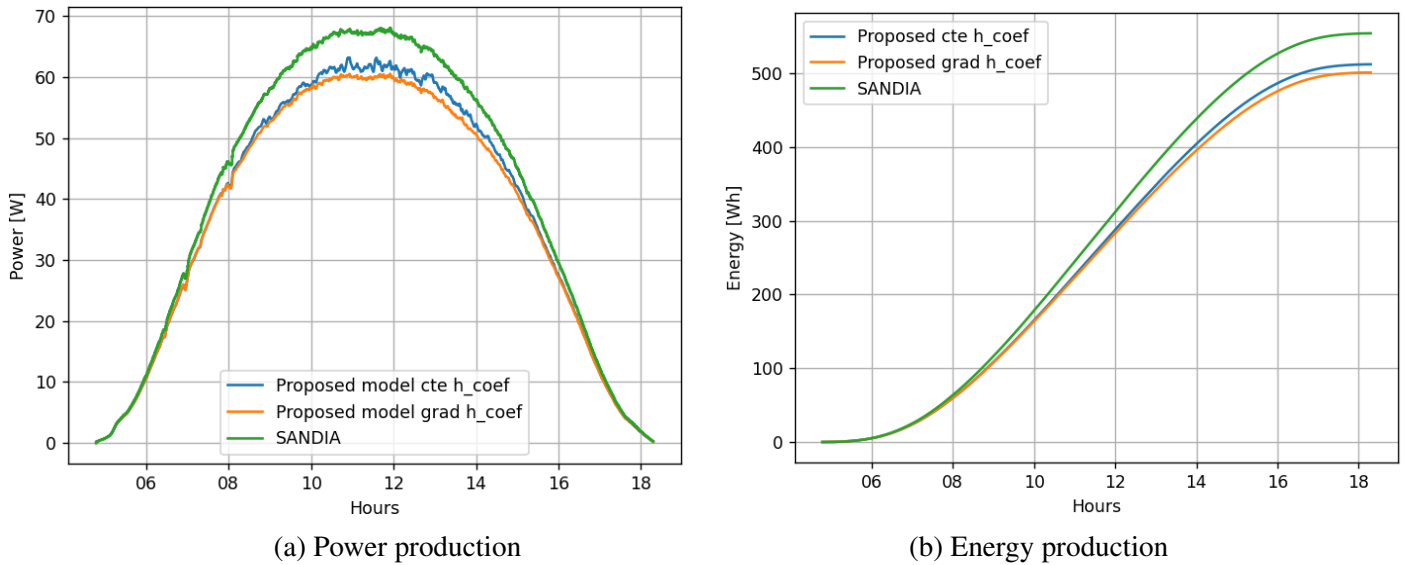
(a) Power production   (b) Energy production

Figure 5: A simulation using meteo field data as inputs. (a) power profile, (b) energy profile.

4. Conclusion

The proposed model is a dynamic thermal model that includes all thermal exchange modes without any linearization of the radiative transfer between the module and its environment, electrical coupling (substring level), and takes spatially resolved h_{coef} for each cell. It was validated against the well-known dynamic SANDIA model. Both models were tested with field meteorological data and introduced using a constant and gradient h_{coef}. A temperature difference is observed between all models, hinting at the necessity of using a spatially resolved thermal model. Indeed, the proposed model underlines the importance of the inclusion of the convective boundary condition in a thermal model for PV installations. The existence of the boundary layer puts some PV cells at a lower working point, hindering the entire module's electrical production. The finality of this work will be the starting point for an upcoming aerodynamic model where its output will be h_{coef} distribution for a more accurate thermo-electric coupling. Thus, the proposed model fills this gap by creating the groundwork for the h_{coef} inhomogeneity on PV modules. The next steps are the development of an aerodynamic model to calculate the h_{coef} with more precision, where it can be extracted using CFD simulation, and upgrading the internal models, such as the electrical model.

References

[1] T.J. Dijkman and R.M.J. Benders. "Comparison of Renewable Fuels Based on Their Land Use Using Energy Densities". In: *Renewable and Sustainable Energy Reviews* 14.9 (Dec. 2010), pp. 3148–3155.

[2] Aritra Ghosh. "A Comprehensive Review of Water Based PV: Flotavoltaics, under Water, Offshore & Canal Top". In: *Ocean Engineering* 281 (Aug. 2023), p. 115044.

[3] Aritra Ghosh. "Nexus between Agriculture and Photovoltaics (Agrivoltaics, Agriphotovoltaics) for Sustainable Development Goal: A Review". In: *Solar Energy* 266 (Dec. 2023), p. 112146.

[4] IEA IRENA UNSD World Bank WHO. *Tracking SDG 7: The Energy Progress Report*. World Bank, Washington DC. © World Bank of Melbourne, 2023.

[5]   Leonardo Micheli. "The Temperature of Floating Photovoltaics: Case Studies, Models and Recent Findings". In: *Solar Energy* 242 (Aug. 2022), pp. 234–245.

[6]   Md Atiqur Rahaman et al. "Floating Photovoltaic Module Temperature Estimation: Modeling and Comparison". In: *Renewable Energy* 208 (May 2023), pp. 162–180.

[7]   Yujian Gong et al. "TVACPSO-assisted Analysis of the Effects of Temperature and Irradiance on the PV Module Performances". In: *Energy* 227 (July 2021), p. 120390.

[8]   A. Senturk and R. Eke. "A New Method to Simulate Photovoltaic Performance of Crystalline Silicon Photovoltaic Modules Based on Datasheet Values". In: *Renewable Energy* 103 (Apr. 2017), pp. 58–69.

[9]   Martin K Fuentes. "' A Simplified Thermal Model for Flat-Plate Photovoltaic Arrays". In: *United States Department of Energy* (1987).

[10]   S. Armstrong and W.G. Hurley. "A Thermal Model for Photovoltaic Panels under Varying Atmospheric Conditions". In: *Applied Thermal Engineering* 30.11-12 (Aug. 2010), pp. 1488–1495.

[11]   Diego Torres-Lobera and Seppo Valkealahti. "Inclusive Dynamic Thermal and Electric Simulation Model of Solar PV Systems under Varying Atmospheric Conditions". In: *Solar Energy* 105 (July 2014), pp. 632–647.

[12]   German Osma-Pinto and Gabriel Ordóñez-Plata. "Dynamic Thermal Modelling for the Prediction of the Operating Temperature of a PV Panel with an Integrated Cooling System". In: *Renewable Energy* 152 (June 2020), pp. 1041–1054.

[13]   Giuseppe Marco Tina, Fausto Bontempo Scavo, and Antonio Gagliano. "Multilayer Thermal Model for Evaluating the Performances of Monofacial and Bifacial Photovoltaic Modules". In: *IEEE Journal of Photovoltaics* 10.4 (July 2020), pp. 1035–1043.

[14]   Giuseppe Marco Tina et al. "Analysis of Water Environment on the Performances of Floating Photovoltaic Plants". In: *Renewable Energy* 175 (Sept. 2021), pp. 281–295.

[15]   Bert Herteleer et al. "Investigating Methods to Improve Photovoltaic Thermal Models at Second-to-Minute Timescales". In: *Solar Energy* (Dec. 2022).

[16]   Matthew Prilliman et al. "Technoeconomic Analysis of Changing PV Array Convective Cooling Through Changing Array Spacing". In: *IEEE Journal of Photovoltaics* 12.6 (Nov. 2022), pp. 1586–1592.

[17]   Sarah E. Smith et al. "Increased Panel Height Enhances Cooling for Photovoltaic Solar Farms". In: *Applied Energy* 325 (Nov. 2022), p. 119819.

[18]   Chowdhury Mohammad Jubayer, Kamran Siddiqui, and Horia Hangan. "CFD Analysis of Convective Heat Transfer from Ground Mounted Solar Panels". In: *Solar Energy* 133 (Aug. 2016), pp. 556–566.

[19]   Anton Driesse, Joshua Stein, and Marios Theristis. *Improving Common PV Module Temperature Models by Incorporating Radiative Losses to the Sky*. Tech. rep. SAND2022-11604, 1884890, 709196. Aug. 2022, SAND2022–11604, 1884890, 709196.

[20]   A D Jones and C P Underwood. "A thermal model for photovoltaic systems". In: *Solar Energy* 70 (2001), pp. 349–359.